Abdom Imaging 25:607–614 (2000)
DOI: 10.1007/s002610000076

Abdominal Imaging

Multiphase helical CT findings after percutaneous ablation procedures for hepatocellular carcinoma

O. Catalano,[1] **M. Esposito,**[1] **A. Nunziata,**[2] **A. Siani**[1]

[1]Department of Radiology, S. Maria delle Grazie Hospital, via Domitiana loc. La Schiana, Pozzuoli, Naples, I-80078, Italy
[2]Department of Diagnostic Imaging, PSI Napoli EST, via Ciccarelli 1, Naples, I-80147, Italy

Received: 6 April 2000/Accepted: 3 May 2000

Abstract
Background: Multiple-phase helical computed tomography (CT) has been regarded as the method of choice in the evaluation of patients with hepatocellular carcinoma (HCC) treated by nonsurgical procedures. The aim of this article was to report our experience in the assessment of nodular and parenchymal changes recognizable after various percutaneous ablation therapies.
Methods: We reviewed the studies of 116 consecutive patients with HCC treated with multisession percutaneous ethanol injection (56 patients, 98 nodules), single-session percutaneous ethanol injection (14 patients, 31 nodules), radiofrequency thermal ablation (32 patients, 48 nodules), and interstitial laser photocoagulation (14 patients, 25 nodules). CT had been performed 3–28 days after the last session (mean = 18 days) with unenhanced helical acquisition and with contrast-enhanced double- or triple-phase helical acquisition.
Results: Persisting neoplastic tissue was identified within 54.5% of the nodules. It was located centrally in 4.5% of these nodules, peripherally in 11%, and eccentrically in 84.5%, and its shape was crescent in 58%, globular in 24.5%, and other in 16%. On arterial phase scans, viable tumor was hyperdense in 97% of the lesions and isodense in 3%; on portal phase scans, the tumor was hyperdense in 20%, isodense in 28%, and hypodense in 52%; on delayed phase scans, the tumor was consistently hypodense. Tumor necrosis was always hypodense on contrast-enhanced scans. On unenhanced images, 7.4% of the nodules were undetectable. Nodule diameter appeared as unchanged in 53% of the nodules and as larger in 47%; its shape was unchanged in 54% and modified in 46%; its margins were unchanged in 36% and modified in 64%. A rim of granulation tissue was detected around 15% of the nodules, and a perilesional transient attenuation difference was detected in 21%. Perihepatic effusion was seen in 13% of the patients, segmental biliary duct dilation and local atrophy each in 9%, arterioportal fistula in 6%, portal vein thrombosis, subcapsular collection and pleural effusion each in 7%, hepatic infarction in 5%, and inferior vena cava thrombosis in 2%.
Conclusion: Percutaneous ablation of HCC may cause several changes. Knowledge of their CT appearance is mandatory to correctly assess and manage this tumor.

Key words: Liver—Hepatocellular carcinoma—Percutaneous ethanol injection—Radiofrequency thermal ablation—Interstitial laser photocoagulation—Helical CT—Follow-up.

Local treatment of unresectable hepatocellular carcinoma (HCC) has become a well-established approach. Several imaging-guided procedures have been proposed that may be performed percutaneously, but in some cases these procedures may be performed intraoperatively or during laparoscopy: multisession ethanol injection (MS-PEI) therapy [1–3], single-session ethanol injection (SS-PEI, or "one-shot") therapy [4], radiofrequency thermal ablation (RFTA) therapy [5–10], interstitial laser photocoagulation (ILP) therapy [11], mitoxantrone injection therapy [12], microwave coagulation therapy [13–16], acetic acid injection therapy [17], hot saline injection therapy [18], and cryoablation therapy [19]. These options may also be performed during a hepatic inflow or outflow occlusion, may be combined with an intraarterial transcatheter chemoembolization, or may follow one another over time [6, 11, 19–22].

Aside from the procedure employed, the posttreatment assessment should focus on the same points: necro-

Correspondence to: O. Catalano

sis, viable tissue persistence, complications, and tumor recurrence [1, 22]. An understanding of the normal and abnormal appearances of percutaneously treated nodules is essential. We analyze the spectrum of changes recognizable within the treated nodule and the host parenchyma by using multiple-phase helical computed tomography (CT) in 116 patients with HCC who had undergone a variety of percutaneous ablation procedures.

Materials and methods

Between December 1996 and October 1999, we evaluated 116 consecutive patients (68 male, 48 female; age range = 38–76 years, mean = 56 years) treated for HCC with percutaneous therapies: 202 nodules (one to five per patient, mean = 1.9) with a larger diameter ranging from 1 to 8 cm (mean = 4.2 cm).

Patients underwent MS-PEI (56 patients, 98 nodules, mean diameter = 2.8 cm), SS-PEI (14 patients, 31 nodules, mean diameter = 4.6 cm), cooled-tip electrode and expandable electrode RFTA (32 patients, 48 nodules, mean diameter = 3.8 cm), and Nd-YAG laser ILP (14 patients, 25 nodules, mean diameter = 4.1 cm).

CT was performed 3–28 days after the last session (mean = 18 days) with a Somatom Plus 4 unit (Siemens AG, Erlangen, Germany). Unenhanced images were obtained in all subjects: volumetric acquisition, 8–10-mm collimation, pitch 1, 5–8-mm reconstruction interval. Contrast-enhanced images were obtained with double-phase volumetric acquisition (arterial and portal) in 28 cases, triple-phase volumetric acquisition (arterial, portal, and delayed) in 48, and double-phase volumetric acquisition plus targeted delayed scans in 40: 8-mm collimation, pitch 1, 5-mm reconstruction interval. A nonionic contrast medium (iomeprol 350 mgI/mL, Iomeron, Bracco, Milan, Italy) was administered through a 16–18-gauge needle and a power injector (Angiomat 6000, Liebel-Flarsheim, Cincinnati, OH). A volume of 135 mL was given at 4 mL/s. Acquisition delay was 25 s, 60–75 s, and 110 s, respectively.

Serial studies were performed in patients with residual tumor tissue; additional treatments with subsequent CT evaluation were performed in 39 of our cases: 20 were studied three times, 13 four times, and six five times. In this study we reviewed only the CT findings recognizable after the first treatment.

We retrospectively assessed the following nodular changes: larger diameter, global shape, borders, gas formation, necrosis (defined as the nonenhancing portion), and viable tumor tissue presence (defined as the portion with persistent arterial phase enhancement), extension (100%, >75%, >50%, >25%, or <25%), location (central, peripheral circumferential, or peripheral eccentric), and shape (crescent, globular, or other).

We also analyzed the parenchymal changes: peripheral granulation tissue (defined as a thin rim of slightly hyperattenuating tissue detectable on all phases), peritumoral transient attenuation difference (THAD; defined as a non-nodular, arterial phase hyperattenuation without a clear equivalent on the other phases), arterioportal fistula (defined as early venous opacification with or without THAD), intrahepatic biliary tract dilation, portal vein or inferior vena cava thrombosis (defined as nonenhancing filling defect), subsegmental atrophy (defined as a paratumoral capsular concavity), subcapsular paratumoral effusion, perihepatic effusion, and pleural effusion.

Results

Tumor changes are summarized in Table 1.

Table 1. Nodular changes[a]

	MS-PEI	SS-PEI	RFTA	ILP	Total
Patients	56	14	32	14	106
Nodules	98	31	48	25	202
	n (%)	*n* (%)	*n* (%)	*n* (%)	*n* (%)
Volume					
Unchanged	70 (71.4)	9 (29)	20 (41.7)	8 (32)	107 (53)
Increased	28 (28.6)	22 (71)	28 (58.3)	17 (68)	95 (47)
Shape					
Unchanged	77 (78.6)	12 (38.7)	10 (20.8)	10 (40)	109 (54)
Modified	21 (21.4)	19 (61.3)	38 (79.2)	15 (60)	93 (46)
Borders					
Unchanged	46 (46.9)	7 (22.6)	9 (18.7)	10 (40)	72 (35.5)
Modified	52 (53)	24 (77.4)	39 (81.3)	15 (60)	130 (64.4)
Well defined	60 (61.2)	27 (87)	41 (85.4)	20 (80)	148 (73.3)
Poorly defined	38 (38.8)	4 (12.9)	7 (14.6)	5 (20)	54 (26.7)
Residual tumor					
100%	3 (3)	—	—	1 (4)	4 (2)
>75%	6 (6.1)	—	—	—	6 (3)
>50%	10 (10.2)	1 (3.2)	—	2 (8)	13 (6.4)
>25%	11 (11.2)	6 (19.4)	6 (12.5)	10 (40)	33 (16.3)
<25%	23 (23.5)	14 (45.2)	11 (22.9)	6 (24)	54 (26.7)
Absent	45 (45.9)	10 (32.3)	31 (64.6)	6 (24)	92 (45.5)
Granulation rim	10 (10.2)	8 (25.8)	10 (20.8)	4 (16)	32 (15.2)
Peritumoral THAD	15 (15.3)	4 (12.9)	16 (33.3)	8 (32)	43 (21.3)

[a] Percentages refer to the number of nodules treated with each technique

Necrosis always showed low attenuation on contrast-enhanced scans. Hypodensity (necrosis-to-parenchyma gradient) was more marked on delayed phase images than on portal and arterial phase scans. On unenhanced scans, 15 nodules (7.4%) were isodense (undetectable).

Residual tumor tissue was identified within 110 of 202 nodules. It was located centrally in five of these (4.5%), peripherally in 12 (10.9%), and eccentrically in 93 (84.5%). The shape was crescent in 64 lesions (58.2%), globular in 27 (24.5%), and different in 19 (16.4%).

On images acquired during arterial phase, the residual tumor was hyperdense in 107 lesions (97.3%) and isodense in three (2.7%). On portal phase images, it was hyperdense in 22 nodules (20%), isodense in 31 (28.2%), and hypodense in 57 (51.8%). On delayed phase images, it was always hypodense (100%).

Tumor diameter appeared as unchanged in 107 of 202 nodules and as larger in 95. Its shape was unchanged in 109 cases and modified in 93, resulting as rounder or as more oval or even oblong. The margins were unchanged in 72 lesions and modified in 130, usually appearing as clearer and defined.

Intranodular gas bubbles were detected in 18 nodules (8.9%; especially in subjects treated with SS-PEI and ILP). A hypodense line due to necrosis alongside the needle or electrode tract was recognizable in 12 lesions (5.9%). A rim of granulation tissue was detected in 32

Table 2. Parenchymal changes[a]

	MS-PEI	SS-PEI	RFTA	ILP	TOTAL
Patients	56	14	32	14	106
Nodules	98	31	48	25	202
	n (%)	*n* (%)	*n* (%)	*n* (%)	*n* (%)
Arterioportal fistula	1 (1.8)	2 (14.3)	1 (3.1)	2 (14.3)	6 (5.7)
Hepatic infarction	1 (1.8)	2 (14.3)	—	2 (14.3)	5 (4.7)
Portal thrombosis	3 (5.4)	2 (14.3)	2 (6.2)	—	7 (6.6)
Caval thrombosis	1 (1.8)	—	—	1 (7.1)	2 (1.9)
Biliary duct dilation	4 (7.1)	3 (21.4)	2 (6.2)	1 (7.1)	10 (9.4)
Local atrophy	1 (1.8)	4 (28.6)	3 (9.4)	2 (14.3)	10 (9.4)
Subcapsular collection	1 (1.8)	2 (14.3)	2 (6.2)	2 (14.3)	7 (6.6)
Perihepatic fluid	3 (5.4)	4 (28.6)	3 (9.4)	4 (28.6)	14 (13.2)
Pleural fluid	2 (3.6)	2 (14.3)	2 (6.2)	1 (7.1)	7 (6.6)

[a] Percentages refer to the number of patients treated with each technique

nodules, mainly after MS-PEI and RFTA, and a perilesional THAD in 43, particularly after RFTA and ILP.

Parenchymal changes are listed in Table 2. An arterioportal fistula was recognized in six of 106 patients (especially after SS-PEI and ILP), hepatic infarction in five, segmental biliary tract dilation in 10 (mainly after MS-PEI and SS-PEI), portal vein thrombosis in seven, inferior vena cava thrombosis in two, local atrophy in 10, subcapsular collection in seven, perihepatic effusion in 14, and right pleural effusion in seven.

Discussion

Contrast-enhanced helical CT has gained a central role in the detection, staging, and posttreatment evaluation of HCC [6, 23–26]. It allows rapid scanning of the entire liver during the various phases of contrast enhancement, thereby providing information about the changes within the treated nodule and the surrounding parenchyma. Lesion-to-liver contrast and conspicuity of all findings are increased when compared with nonhelical CT studies because more pronounced differences between neoplastic tissue, necrotic tissue, and noncancerous parenchyma can be obtained.

Although the arterial phase acquisition is necessary to recognize enhancing viable tissue, the CT study must be performed with double or triple passage [6, 26]. Tumor necrosis has a higher conspicuity on venous or delayed phase images. Moreover, these phases are helpful in detecting homogeneously necrotic nodules, differentiating tumor persistence from inflammatory reaction and THAD areas, and recognizing complications such as venous thrombosis.

When an MS-PEI therapy or a percutaneous mitoxantrone injection therapy is performed, CT is usually obtained 20–30 days after the last session [1–3, 12]. Other treatments such as SS-PEI, RFTA, hot saline injection, acetic acid injection, ILP, and microwave coagulation require a shorter follow-up, and patients undergo CT 5–15 days after treatment and eventually repeat the study 1–2 months later [4–6, 11, 18].

CT demonstration of treatment effectiveness is fundamental for patient management and prognosis. In subjects eligible for radical management (patients in Child–Pugh class A or B with uni- or multinodular nonadvanced HCC and without evidence of vascular invasion or extrahepatic metastases), demonstration of incomplete necrosis requires a new treatment, with the same or other modality; local recurrence is rare if complete ablation has been achieved, but regrowth is frequent if even a small amount of tumor cells has been left in place [1, 27, 28].

Knowledge of all nodular and parenchymal changes detectable after the variety of ablation procedures currently used is relevant to understand treatment mechanism and to avoid pitfalls. Recognition of complications is mandatory to correctly manage the injury and to avoid further damage during other sessions.

Tumor changes

The necrotic tissue appears as hypodense on almost all scans, regardless of its pretreatment appearance (Figs. 1, 2). In our series the successfully ablated nodule resulted as isoattenuating or, more frequently, as hypoattenuating on unenhanced images and usually showed a greater conspicuity when compared with the pretreatment appearance, as has been described in the literature [2, 6, 17, 26, 29–31].

On contrast-enhanced images, necrosis was always hypoattenuating, and its conspicuity was usually greater on delayed than on venous phase acquisition or on arterial phase acquisition.

Several homogeneously necrotic lesions were barely appreciable on arterial phase acquisition and were recognized only because of comparison with the other images. All lesions were seen on at least one helical acquisition. In the series by Ebara et al. [29], 15% of the nodules were undetected on pretreatment nonhelical CT and 22% were undetected 3 months after PEI. In our retrospective analysis, we could not evaluate the attenuation values of the ablated tissue. Nevertheless, we noted that nodules treated by MS-PEI were less hypodense than those treated with other methods. This may reflect the prevalent coagulation necrosis achieved with ethanol and the prevalent liquefactive necrosis obtained with other procedures [1, 9, 26, 30].

Persistent tumor was hyperattenuating (hypervascular) on arterial phase acquisition when compared with both the surrounding parenchyma and the necrotic component; usually the conspicuity of this tissue was relevant and the appearance was similar to the usual pretreatment findings (Figs. 3–5). In only three nodules, the residual

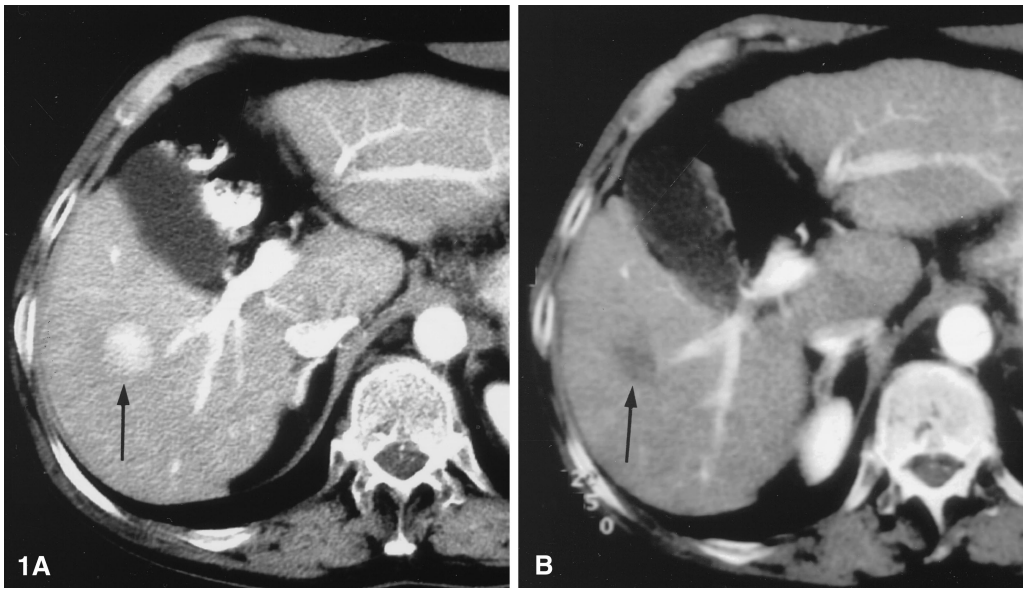

Fig. 1. A Arterial phase CT image. Enhancing hepatic nodule (*arrow*). **B** Arterial phase CT image 23 days after MS-PEI. Necrotic, poorly defined nodule (*arrow*).

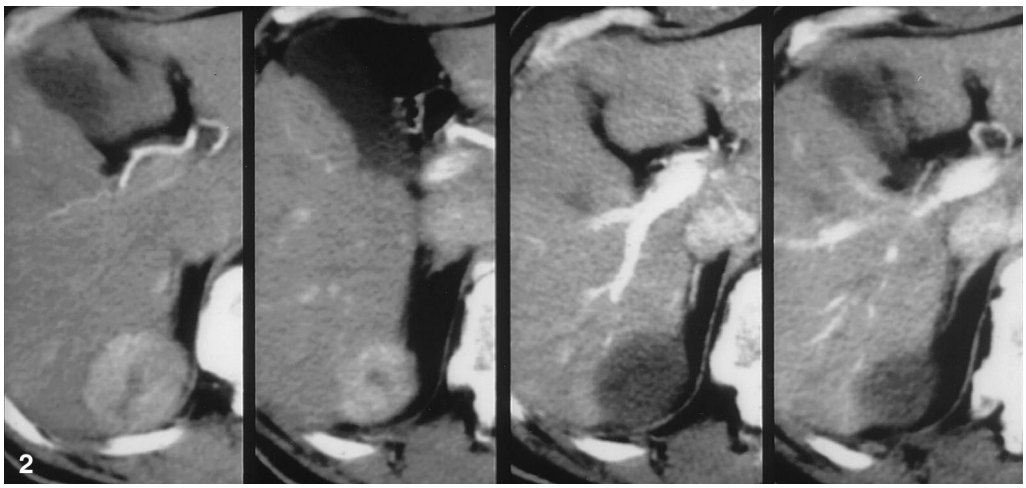

Fig. 2. Arterial-phase CT images before (left) and after (right) RFTA therapy. The hypervascular liver tumor is homogeneously hypoattenuating (necrotic) after treatment.

tissue appeared as isodense, but its persistence was clear because of its large dimension.

On portal phase acquisition, the cancerous tissue was in most cases hypoattenuating with respect to the parenchyma but more attenuating than the necrotic portion; in some cases, it was isodense or even slightly hyperdense in relation to the hepatic parenchyma. On delayed phase acquisition, the residual cancer was always hypodense in comparison with the parenchyma, although less than the necrotic tissue. After all, the pattern through all phases was similar to that of native HCC [23–25].

The residual tissue was located in most cases peripherally, with a crescent or, less frequently, a globular shape. Marginal ablation is a key point: alcohol spreading during PEI may be incomplete in the tumor edge [1], and vessel proximity may prevent complete necrosis with RFTA and microwave coagulation and with cryoablation because of tissue cooling and of a heat sink effect [9, 19, 26, 31]. In patients treated with cryosurgery, for example, a "cuff" of normal parenchyma has been observed around larger peritumoral vessels [32].

We also noted that the persistent tissue was frequently located along the opposite side from the percutaneous access and/or in proximity with large peritumoral vessels. Both of these findings can be easily understood: the innermost cancer tissue is more difficult to be reached by the needle or electrode, which is usually placed at the center of the mass, whereas the most superficial portion can be ablated while withdrawing the tool. The operator is usually careful in placing the needle or electrode deep

Fig. 3. Arterial phase CT image. Deeply located, peripheral area of viable tumor tissue (*arrow*) 14 days after RFTA therapy. Mild perihepatic effusion.

Fig. 4. Arterial phase CT image. Deep, enhancing area of residual tumor (*arrows*) 17 days after ILP therapy. Small intranodular gas bubbles are recognizable on the right.

Fig. 5. A Arterial phase CT image. Crescent area of partial residual tumor (*arrow*) after MS-PEI. **B** Arterial phase CT image. Homogeneous necrosis after nodule retreatment with MS-PEI.

within the liver and is afraid to damage large vascular or biliary structures; the protective effect of perinodular vessels has already been mentioned.

In a few cases the residual tumor after PEI was detected centrally, bridging side to side. This was probably due to intranodular septa that may have prevented alcohol diffusion [1].

In most of our cases the residual tumor appeared typically as an eccentric, crescentlike area with deep location and irregular borders that showed early phase enhancement and portal and delayed phase hypodensity. This pattern usually allowed a correct interpretation and a differentiation from perinodular perfusion abnormalities, iatrogenic arteriovenous fistulas, and reactive granulation tissue.

If compared with the pretreatment scans, the HCC nodule may appear unchanged in both volume and shape.

In the early assessment, the diameter may result as not modified or increased. The latter occurrence testifies to a more radical effect at the level of perinodular tissue; complete marginal ablation and prophylaxis toward regrowth are predictable. We observed this feature espe-

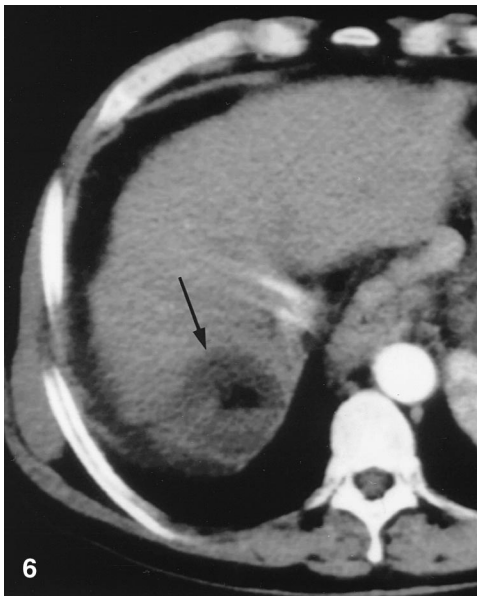

Fig. 6. Arterial phase CT image. Homogeneously necrotic area 20 days after RFTA treatment (*arrow*). Air lucencies are visible within the tumor. Mild peritoneal effusion.

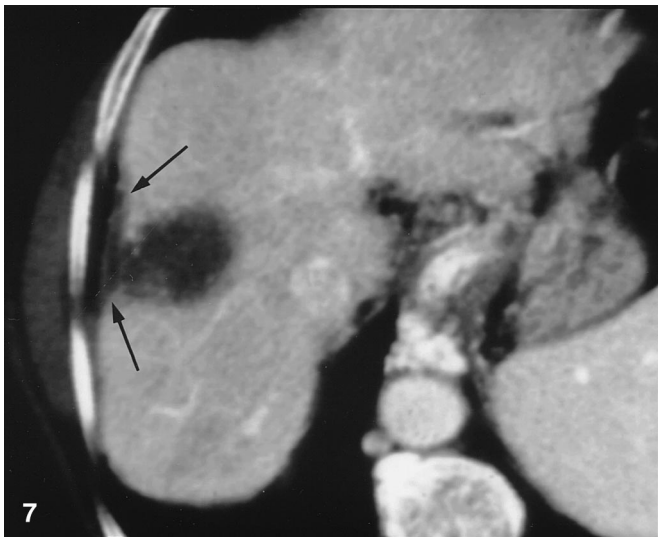

Fig. 7. Portal phase CT image. Hypodense, necrotic nodule after MS-PEI, partly adjacent to the liver capsule. Mild retraction of the contiguous liver surface with a thin subcapsular collection (*arrows*).

cially after RFTA (moderate) and after ILP and SS-PEI (more evident). Obviously, size increases after treatment should be limited.

The shape is often unchanged. Sometimes it results as rounder and with more regular borders when compared with its pretreatment appearance. In other cases, the shape becomes oblong, especially in the direction of the percutaneous access path. We mainly detected slightly oblong lesions after RFTA, although we never identified the tear-drop shape reported in patients treated with percutaneous microwave coagulation [31] or with cryosurgery [32] and the crescent shape observed after acetic acid injection [17].

The borders usually appeared as more defined and regular, especially after SS-PEI, RFTA, and ILP. In our series, irregular edges correlated in most cases with the location and extension of residual viable tissue.

Several nodules also showed one or more border indentations. This appearance was noted only after ILP and, in our opinion, reflected the position of the needle. Multiple indentations were seen in larger lesions, usually treated with a multipolar approach.

Small gas bubbles within the treated nodule result from tissue necrosis (Fig. 6) and are especially detected if the CT study is performed during the first days after treatment and when microwave coagulation [26], acetic acid injection [17], cryosurgery [32, 33], ILP [34], or SS-PEI [4] has been performed. Instead, intranodular air densities are usually not recognized after MS-PEI [29, 35], even in the series by Joseph et al. [36], where scans were obtained immediately after CT-guided PEI, and in the series by Yoshikawa et al. [35], where CT was performed 2–14 days after treatment. Instead, we observed this finding in patients treated with RFTA, a feature detected by some investigators [7] but not by others [9]. Sometimes gas densities may even be found within the contiguous portal branches [4, 34].

After microwave coagulation, Mitsuzaki et al. [26] recognized an air content in 19% of the lesions treated intraoperatively but in none treated percutaneously. On aspiration, four lesions proved to be abscesses. We never sampled the intralesional fluid, but in our series there was always a nominal amount of gas and no patient showed clinical or laboratory signs of sepsis.

After microwave coagulation [26] and after cryosurgery [32], all lesions, regardless of the depth of the treated tumor, are attached to the liver capsule, a feature rarely recognized in our series.

Parenchymal changes and complications

The needle or electrode path can often be recognized as one or more hypodense bands extending from the liver surface to the nodule. In our series, it was detected mainly in patients treated with ILP and was better appreciable in proximity to the nodule. After ILP and RFTA, the tool is usually withdrawn while still warm to cauterize the tract and prevent tumor seeding, and this may cause the minimum necrosis detected on our CT scans.

A thin marginal rim of enhancement can be identified when CT is performed 1–2 months after the percutaneous

procedure [9, 29]. In our series, this granulation halo was relatively uncommon (15%) and was appreciable after all modes of treatment. It can be distinguished from viable tissue because of slight hyperattenuation on all phases, its symmetrical and almost circumferential distribution, and thinness. Additional CT studies may demonstrate regression of this inflammatory rim.

A perinodular area of THAD should not be confused with the previous finding and should be regarded as a frequent CT and also magnetic resonance imaging feature of early posttreatment period, particularly after SS-PEI, microwave coagulation, cryosurgery, RFTA, and ILP [1, 6, 9, 14, 26, 32, 33, 37]. This transient hyperattenuation (increased arterial-related enhancement) is due to reactive hyperemia, decreased portal flow, or thrombosis of portal branches, and is usually ringlike or wedge-shaped (extending from the tumor to the liver capsule) [1, 26, 37].

Yoshikawa et al. [35] detected high-attenuation areas around 33% of the lesions treated with MS-PEI, and Kuszyk et al. [32] detected such areas around 54% of the lesions ablated with cryosurgery. The relatively low rate of detection in our series is due to the time intervening from treatment because perilesional THAD disappears 2–3 months after the percutaneous procedure [1, 26]. In our experience, this transient perifocal hyperattenuation can easily be distinguished from residual tumor because of its absence on pretreatment study and because of its isodensity on portal and delayed phase images. Follow-up CT will usually show regression of this feature.

Iatrogenic arterioportal fistulas also appear as transient hyperattenuating areas, sometimes with early opacification of small veins internally [38, 39]. Macroscopic fistulas close to the nodule are difficult to distinguish from viable tissue because of similar contrast enhancement. In our experience, this is the main pitfall in assessing the ablated HCC.

Segmental mild dilatation of the biliary ducts has been found in 8% of the subjects treated by MS-PEI [35] and there was a similar overall prevalence in our series. We detected this finding mainly in subjects treated with SS-PEI. Although biliary wall damage is considered a serious risk during RFTA [9], only 6% of our patients treated with this option showed a dilatation of the intrahepatic bile duct and none developed a biloma.

Small subcapsular effusion may be identified at the level of the access surface. A limited perihepatic effusion is possible, often localized in proximity to superficial lesions. Uncommonly, a mild right pleural effusion with basal consolidation may also develop. All these findings are transient.

Thickening of the hepatic surface has also been observed, especially when the tumor is located superficially [6], but this finding was not observed in our series.

Local atrophy appears as a concavity or a retraction of the liver surface close to the nodule (Fig. 7). It has been reported in 40% of the nodules treated with MS-PEI [35] but is a late change. In 9% of our cases, we noted a capsular retraction, especially when relevant necrosis involved large peripheral tumors and when peripheral infarctions developed as a consequence of the percutaneous procedure.

Treatment of lesions in segments II–III and VI led to distal segmental or subsegmental infarction in five of our cases. Hepatic infarction is recognizable as a constantly nonenhancing area with a poorly or well-defined edge; the shape may be cuneiform, and a capsular enhancing rim may be identified.

Venous thrombosis after PEI is due to direct ethanol spread and may be reversible [1]. The portal branches or the extrahepatic portal vein are usually involved. In our series, there were seven portal thromboses. Of these, two were within the left portal branch and five were within segmental vessels. The intrahepatic inferior vena cava may be damaged, as in two of our patients, one with segment I HCC and another with segment V HCC and large intrahepatic fistula.

In conclusion, each percutaneous procedure carries different and rather peculiar helical CT features, and one may frequently predict the ablation technique performed from the spectrum of findings detected. The two main variables involved in determining these changes were, in our experience, the procedure employed and the time interval between treatment and CT study. SS-PEI, RFTA, and ILP usually cause more clear and dramatic changes within both the tumor and parenchyma. After MS-PEI, all changes are less evident and, consequently, more difficult to be interpreted by the radiologist.

References

1. Bartolozzi C, Lencioni R. Ethanol injection for the treatment of hepatic tumours. *Eur Radiol* 1996;6:682–696
2. Livraghi T, Salmi A, Bolondi L, et al. Small hepatocellular carcinoma: percutaneous ethanol injection. Results in 23 patients. *Radiology* 1988;168:313–317
3. Shiina S, Tagawa K, Unuma T, et al. Percutaneous ethanol injection therapy for the treatment of hepatocellular carcinoma. *AJR* 1990; 154:947–951
4. Livraghi T, Vettori C, Torzilli G, et al. Percutaneous ethanol injection of hepatic tumors: single-session therapy under general anesthesia. *AJR* 1993;160:1065–1069
5. Francica G, Marone G. Ultrasound-guided percutaneous treatment of hepatocellular carcinoma by radiofrequency hypertermia with a "cooled-tip needle". A preliminary clinical experience. *Eur J Ultrasound* 1999;9:145–153
6. Livraghi T, Goldberg SN, Lazzaroni S, et al. Small hepatocellular carcinoma: treatment with radio-frequency ablation versus ethanol injection. *Radiology* 1999;210:655–661
7. McGahan JP, Browning PD, Brock JM, et al. Hepatic ablation using radiofrequency electrocautery. *Invest Radiol* 1990;25:267–270
8. Nagata Y, Hiraoka M, Nishimura Y, et al. Clinical results of radiofrequency hypertermia for malignant liver tumors. *Int J Radiat Oncol Biol Phys* 1997;38:359–365
9. Rossi S, Di Stasi M, Buscarini E, et al. Percutaneous RF interstitial thermal ablation in the treatment of hepatic cancer. *AJR* 1996;167: 759–768

10. Kainuma O, Asano T, Aoyama H, et al. Recurrent hepatocellular carcinoma successfully treated with radiofrequency thermal ablation. *J Hepatobil Pancreat Surg* 1999;6:190–194
11. Heisterkamp J, van Hillerberg R, Ijzermans JN. Interstitial laser coagulation for hepatic tumours. *Br J Surg* 1999;86:293–304
12. Farrés MT, de Baere T, Lagrange C, et al. Percutaneous mitoxantrone injection for primary and secondary liver tumors: preliminary results. *Cardiovasc Intervent Radiol* 1998;21:399–403
13. Seki T, Wakabayashi M, Nakagawa T, et al. Percutaneous microwave coagulation therapy for patients with small hepatocellular carcinoma: comparison with percutaneous ethanol injection therapy. *Cancer* 1999;85:1694–1702
14. Ohmoto K, Miyake I, Tsuduki M, et al. Percutaneous microwave coagulation therapy for unresectable hepatocellular carcinoma. *Hepatogastroenterology* 1999;46:2894–2900
15. Seki T, Wakebayashi M, Nakagawa T, et al. Ultrasonically-guided percutaneous microwave coagulation therapy for small hepatocellular carcinoma. *Cancer* 1994;74:817–825
16. Horigome H, Nomura T, Saso K, et al. Standards for selecting percutaneous ethanol injection therapy or percutaneous microwave coagulation therapy for solitary small hepatocellular carcinoma: consideration of local recurrence. *Am J Gastroenterol* 1999;94:1914–1917
17. Ohnishi K, Yoshioka H, Kosaka K, et al. Treatment of hypervascular small hepatocellular carcinoma with ultrasound-guided percutaneous acetic acid injection: comparison with transcatheter arterial embolization. *Am J Gastroenterol* 1996;91:2574–2579
18. Yoon HK, Song HY, Sung KB, et al. Percutaneous hot saline injection therapy: effectiveness in large hepatocellular carcinoma. *J Vasc Intervent Radiol* 1999;10:477–482
19. Wong WS, Patel SC, Cruz FS, et al. Cryosurgery as a treatment for advanced stage hepatocellular carcinoma: results, complications, and alcohol ablation. *Cancer* 1998;82:1268–1278
20. Tanaka K, Naakamura S, Numata K, et al. Hepatocellular carcinoma: treatment with percutaneous ethanol injection and transcatheter arterial embolization. *Radiology* 1992;185:457–460
21. Buscarini L, Buscarini E, Di Stasi M, et al. Percutaneous radiofrequency thermal ablation combined with transcatheter arterial embolization in the treatment of large hepatocellular carcinoma. *Ultraschall Med* 1999;20:47–53
22. Okada S. Local ablation therapy for hepatocellular carcinoma. *Semin Liver Dis* 1999;19:323–328
23. Baron RL, Oliver JH III, Dodd GD, et al. Hepatocellular carcinoma: evaluation with biphasic, contrast-enhanced, helical CT. *Radiology* 1996;199:505–511
24. Hwang GJ, Kim M-J, Yoo HS, et al. Nodular hepatocellular carcinomas: detection with arterial-, portal-, and delayed-phase images at spiral CT. *Radiology* 1997;202:383–388
25. Kim T, Murakami T, Takahashi S, et al. Optimal phases of dynamic CT for detecting hepatocellular carcinoma: evaluation of unenhanced and triple-phase images. *Abdom Imaging* 1999;24:473–480
26. Mitsuzaki K, Yamashita Y, Nishiharu T, et al. CT appearance of hepatic tumors after microwave coagulation therapy. *AJR* 1998;171:1397–1403
27. Castellano L, Calandra M, Del Vecchio Blanco C, et al. Predictive factors of survival and intrahepatic recurrence of hepatocellular carcinoma in cirrhosis after percutaneous ethanol injection: analysis of 71 patients. *J Hepatol* 1997;27:862–870
28. Hasegawa S, Yamasaki N, Hiwaki T, et al. Factors that predict intrahepatic recurrence of hepatocellular carcinoma in 81 patients initially treated by percutaneous ethanol injection. *Cancer* 1999;86:1682–1690
29. Ebara M, Kita K, Sugiura N, et al. Therapeutic effect of percutaneous ethanol injection on small hepatocellular carcinoma: evaluation with CT. *Radiology* 1995;195:371–377
30. Lencioni R, Caramella D, Bartolozzi C. Response of hepatocellular carcinoma to percutaneous ethanol injection: CT and MR evaluation. *J Comput Assist Tomogr* 1993;17:723–729
31. Hyodoh H, Hyodoh K, Takahashi K, et al. Microwave coagulation therapy of hepatomas: CT and MR appearance after therapy. *J Magn Reson Imaging* 1998;8:451–458
32. Malone DE, Lesiuk L, Brady A, et al. Hepatic interstitial laser photocoagulation: demonstration and possible clinical significance of intravascular gas. *Radiology* 1994;193:233–237
33. Brewer WH, Austin RS, Capps GW, et al. Intraoperative monitoring and postoperative imaging of hepatic cryosurgery. *Semin Surg Oncol* 1998;14:129–155
34. Kuszyk BS, Choti MA, Urban BA, et al. Hepatic tumors treated by cryosurgery: normal CT appearance. *AJR* 1996;166:363–367
35. Yoshikawa J, Matsui O, Kadoya M, et al. Hepatocellular carcinoma: CT appearance of parenchymal changes after percutaneous ethanol injection therapy. *Radiology* 1995;194:107–111
36. Joseph FB, Baumgartner DA, Bernardino ME. Hepatocellular carcinoma: CT appearance after percutaneous ethanol ablation therapy. *Radiology* 1993;186:553–556
37. Ito K, Honjo K, Fujita T, et al. Enhanced MR imaging of the liver after ethanol treatment of hepatocellular carcinoma: evaluation of areas of hyperperfusion adjacent to the tumor. *AJR* 1995;164:1413–1417
38. Kim TK, Choi BJ, Han JK, et al. Nontumorous arterioportal shunt mimicking hypervascular tumor in cirrhotic liver: two-phase spiral CT findings. *Radiology* 1998;208:597–603
39. Lee SJ, Lim JH, Lee WJ, et al. Transient subsegmental hepatic parenchymal enhancement on dynamic CT: a new sign of postbiopsy arterio-portal shunt. *J Comput Assist Tomogr* 1997;21:355–360